D. 2007 Preliminary Experiment

D-1. Overview of the 2007 preliminary experiment

The 2007 preliminary experiment for B08RDP was conducted from 24 July to 31 August. In addition to the five participating centers of the 2006 experiment (MRI/JMA, NCEP, MSC NMC/CMA and CAMS/CMA), the Austrian Zentral Anstalt fur Meterologie und Geodynamik (ZAMG) newly participated in the project in collaboration with the Meteo France. Intercomparisons of the 36 hour EPS forecast with a horizontal resolution of 15 km were again conducted, and the forecast products were uploaded on the website of the B08RDP in near real time. Specifications of Tier-1 ensemble prediction systems of 6 participants are listed in Table D-1-1.

Table D-1-1. Specifications of Tier-1 EPS of six participating centers in the 2007 experiment.

Participants	Model	IC	IC perturbation	Physical perturbation	LBC
NCEP*	GFS (T106L28)	NCEP Global 3DVAR	Breeding	Multi-model	--
MRI/JMA	JMA-NHM (L40M11)	JMA Regional 4DVAR	Targeted Global SV	non	JMA Regional Forecast
MSC	GEM (L28M16)	MSC Global 4DVAR	Targeted Global SV	Markov chain	MSC Global EPS
ZAMG & Meteo-Fr.	ALANDIN (L37M18)	ECMWF Global 4DVAR	ECMWF Global SV	non	ECMWF Global EPS
NMC/CMA	WRF-ARW (L31M15)	WRF-3DVAR	Breeding	Multi-physics	Global EPS
CAMS/CMA	GRAPES (L31M9)	GRAPES-3DVAR	Breeding	Physical perturbation	Global EPS

*NCEP submitted downscaling of GFS global ensemble prediction in 2007.

Specifications of the 2007 EPS of MRI/JMA are given in Table. D-2-1, compared with specifications of the 2006 EPS. As for the initial perturbation method, global targeted singular vector method (D-4-2) was used, while four perturbation methods (D-4-1, 2, 3, 4) were developed and tested (D-4-5).

Tier-2 case studies using a cloud resolving model were also conducted (see D-8).

D-2. Numerical model for the 2007 experiment

In the 2007 experiment, a new version of the JMA nonhydrostatic model as of May 2007 (NHM; Saito et al., 2007a) was employed as the forecast model, where the turbulent closure model, trigger functions in the Kain-Fritsch convection scheme and the atmospheric radiation scheme were modified. Detail of the new turbulent closure model (Mellor-Yamada-Nakanishi-Niino level 3 closure model) is given in Section F-5. The model domain was enlarged from 221 x 201 grids of the 2006 experiment (Fig. C-2-1) to 232 x 200 grids and slightly shifted westward (Fig. D-2-1). The southwestern corner of the verification domain is no longer embedded in the lateral boundary relaxation layers (24 grids = 360 km).

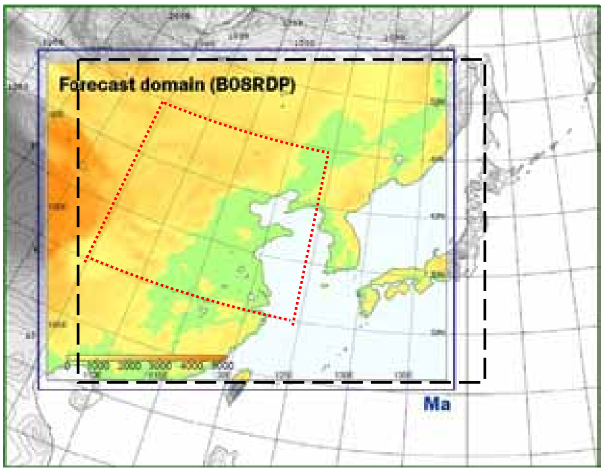

Fig. D-2-1. Domain of the MRI/JMA EPS in the 2007 experiment (solid rectangle). Dashed rectangle indicates domain of the 2006 experiment. Rectangle Ma shows the domain of the Meso 4D-Var (see E-3-1). Fan-shaped dotted sector over east China indicates the domain of the common verification area (105~125°E, 30~45°N).

Table D-2-1. Specifications of the MEP experiments by MRI/JMA in 2006 and 2007.

	2006 Experiment	2007 Experiment
Forecast model	NHM as of March 2006	NHM as of May 2007
Horizontal grid	221×201 (Δx = 15km), Lambert comformal projection	232×200 (Δx = 15km), Lambert comformal projection
Vertical grid	Terrain-following, 40 levels, Δz=40-1180m、 H=22km	No changes
Number of members	11 members	No changes
Initial condition	Initial condition of RSM produced by JMA operational regional 4D-Var (20 km resolution)	JMA operational regional 4D-Var (20 km resolution)
Initial perturbation	JMA one-week global EPS (TL159)	Targeted moist global SV (T63L40)
Lateral boundary	JMA RSM forecast (no perturbation)	No changes
Soil temperatures	4 layer prognostic soil temperatures	4 layer prognostic soil temperatures, Initial perturbations are added

D-3. Initial and boundary conditions for the control run

The operational regional analysis and the forecast of regional model of JMA (RSM) were employed for initial and lateral boundary conditions for the control run respectively. Although these were almost the same as in the 2006 experiment, the initial condition was slightly changed from the initial condition of RSM which includes the nonlinear normal mode initialization in 2006 to the original regional analysis in 2007. To enlarge the EPS model domain westward, enlarged RSM model forecast data were newly produced by NPD/JMA for the B08RDP project and were transferred to MRI in near real time through the exclusive line between MRI and JMA.

Application of Meso 4D-Var analysis to the Beijing area was conducted by way of trial, but it was not employed in the 2007 experiment and implemented in the 2008 experiment (see E-3-1).

D-4. Initial perturbation methods

D-4-1. WEP method

In the 2006 experiment, perturbations from the JMA operational one week global EPS (WEP) were used as the initial perturbation of the mesoscale ensemble prediction. Same method was tested in the 2007 experiment as well for reference. Detailed procedures are the same as described in C-4.

D-4-2. Targeted global singular vector (GSV) method

The targeted global singular vector (GSV) method was adopted to make initial perturbation fields in the 2007 preliminary experiment. The GSV method was developed by the Japan Meteorological Agency (JMA) with the aim of the Typhoon EPS (see section F-2).

An ensemble prediction system (EPS) for mesoscale phenomena in combination with the GSV method (GSV EPS) has been developed by MRI. The model to calculate the SVs was the tangent-linear and its adjoint of the JMA global spectral model (GSM). The model used for the EPS run was the JMA non-hydrostatic model (NHM).

The resolution of the tangent linear global model and its adjoint was T63L40. The model includes moist physical processes. The chosen optimization time of SVs was 24 hours. The SVs were targeted for the Beijing region as defined by the common verification area (30–45°N, 105–125°E). The total energy(TE) norm used in this experiment is equivalent to the moist TE-norm (Barkmeijer et. al., 2001):

$$\begin{aligned} TE &= \frac{1}{2}\int_0^1 \int_S (\nabla\Delta^{-1}\zeta_x \cdot \nabla\Delta^{-1}\zeta_y + \nabla\Delta^{-1}D_x \cdot \nabla\Delta^{-1}D_y + \frac{c_p}{T_r}T_xT_y \\ &+ w_q\frac{L^2}{c_pT_r}q_xq_y)dS\left(\frac{\partial p}{\partial \eta}\right)d\eta + \frac{1}{2}\int_S R_dT_rP_r \ln\pi_x \cdot \ln\pi_y \, dS, \end{aligned} \qquad \text{(D-4-1)}$$

where ζ, D, T, q, $\ln\pi$ being the vorticity, divergence, temperature, specific humidity and logarithm of the surface pressure and c_p is the specific heat at constant pressure, R_d is the gas constant for dry air, L is the latent heat of condensation, $T_r = 300$ K is a reference temperature, $P_r = 800$ hPa is a reference pressure and $w_q = 0.6$ is a constant. The value $w_q = 0.6$ instead of $w_q = 1.0$ was employed in order to increase the initial perturbation energy of specific humidity. The amplitude of the initial perturbation was fixed at the mean value of the estimated standard error of analysis. The normalized perturbations were downscaled into the NHM model planes with the 15-km horizontal grid and 40 layers. The lateral boundaries were not perturbed.

The GSV EPS was applied to a heavy rainfall event occurred in July 2007 in Kyushu, Japan. The operational MSM forecast of JMA failed to predict the intense rainfall. When a 10-km grid is used, a member of the GSV EPS predicted the heavy rainfall area (more than 50 mm/3 hours) with a 24-h lead time (not shown).

D-4-3. Mesoscale singular vector (MSV) method

Singular vectors calculated using coupled tangent linear (TLM) and adjoint (ADM) models are optimum structures for describing perturbation growth over a finite forecast time interval. This method was developed at the European Centre for Medium-Range Weather Forecasts (Buizza et al., 1993) to create a set of initial perturbations for ensemble prediction and for sensitivity analyses of adaptive observations used to improve the initial conditions of their global models. At present, JMA applies global singular vectors (GSVs) to ensemble prediction systems (EPSs) for weekly and typhoon forecasts.

Many natural hazards, however, such as localized heavy rain or wind gusts, are caused by mesoscale disturbances rather than by synoptic-scale systems. Therefore, mesoscale EPSs are attracting attention as a means of providing valid, objective information for disaster prevention. GSVs can be applied to initial mesoscale EPS perturbation by downscaling, but the initial perturbations calculated by this method may not be suitable for mesoscale forecasts because of insufficient horizontal resolution. To achieve adequate resolution in calculating the GSVs, unrealistically huge computer resources are needed. Therefore, in this study, mesoscale singular vectors (MSVs) were calculated, and their potential use in mesoscale EPSs was investigated. In addition, MRI/JMA studied optimization of the initial perturbations by the local ensemble transform Kalman filter (LETKF) (Miyoshi et al., 2006) and mesoscale breeding methods (see sections D-4-4 and E-4-5).

MSVs were calculated using TLM and ADM of the JMA nonhydrostatic model variational data assimilation system (Honda et al., 2005). In TLM and ADM, some parts of the nonlinear model are simplified, such as large-scale condensation and the moisture convective adjustment used in moisture processes. To solve the eigenvalue problem, the Lanczos algorithm (Simon and Parlett, 1980) with Gram-Schmidt re-orthogonalization was adopted.

The total energy norm, including a moisture term (Ehrendorfer et al., 1999) used as a constraint, is

$$\|\mathbf{x}\|^2 = \frac{1}{S}\int_{z_1}^{z_2}\iint_S \frac{1}{2}\rho\left(u'^2 + v'^2 + w'^2 + w_t\frac{C_p(\theta')^2}{\Theta} + RT_r\left(\frac{p'}{p_r}\right)^2 + w_q\frac{L^2}{C_pT_r}q'^2\right)dSdz\,, \tag{D-4-2}$$

where ρ is density; u, v, w are wind components; θ, p, q are potential temperature, pressure, and the mixing ratio of water vapor, respectively; $C_p = 1005.7\ \mathrm{Jkg^{-1}K^{-1}}$ is the specific heat at constant pressure; $\Theta = 300\ \mathrm{K}$, $T_r = 300\ \mathrm{K}$, and $p_r = 10^5\ \mathrm{Pa}$ are the reference values of potential temperature, temperature, and pressure; $R = 287.04\ \mathrm{Jkg^{-1}K^{-1}}$ is the gas constant; $L = 2.51 \times 10^6\ \mathrm{Jkg^{-1}}$ is the latent heat constant; and $w_t = 3.0$ and $w_q = 0.5$ are the weights of the potential temperature and water vapor mixing ratio terms, respectively. These weights were determined such that the composition ratio of individual terms in the initial norm was equivalent to that calculated using standard analysis errors instead of initial perturbations.

The specification of the MSVs for 2007 B08RDP experiment is listed in Table D-4-1. It seems that the optimization time is rather short for 36 hours ensemble forecast, but it is set to 6 hours to ensure the validity of the tangent linear approximation. When moisture physical processes are treated in TLM and ADM, perturbations associated with nonlinearities in the convective parameterization often grow explosively if the forecast time exceeds a certain threshold, depending on the individual case.

Initial perturbations for the ensemble forecasts were made from MSVs with adjustment of their amplitudes. The adjustment was carried out to make the average values of the initial perturbations equivalent to standard analysis errors. Then, standardization was performed not to exceed the limits, $\mathrm{p} = 5.0\ \mathrm{hPa}, (\mathrm{u}, \mathrm{v}) = 6.0\ \mathrm{m/s}, \theta = 4.0\ \mathrm{K}$ and $\mathrm{qv} = 1.5\ \mathrm{g/kg}$. Though lateral boundary perturbation methods for the growth of spreads in a regional model would be worthy of consideration, they were not built into the ensemble forecasting system used in the 2007 experiment.

Preliminary experiments were conducted in 2007 at MRI to compare and examine the performance of some initial perturbation methods and to determine which initial perturbation method to use in the B08RDP 2008 experiment. The ensemble forecasts were performed using the JMA nonhydrostatic model with a 15-km horizontal resolution and 40 vertical levels. The number of ensemble members was 11, including the no-perturbation control forecast.

Table D-4-2 compares singular values, which are equivalent to the linear growth rate during the optimization time, with nonlinear growth rates. The similarity index between linear and nonlinear growth is also shown, defined as

$$\mathrm{SI} = \left(\frac{\mathbf{a}}{\sqrt{(\mathbf{a},\mathbf{a})}}, \frac{\mathbf{b}}{\sqrt{(\mathbf{b},\mathbf{b})}}\right), \tag{D-4-3}$$

$$\mathbf{a} = \mathbf{E}_{\mathrm{f}}^{\frac{1}{2}}\mathbf{M}\mathbf{x}(\mathrm{t}=0)\,, \qquad \mathbf{b} = \mathbf{E}_{\mathrm{f}}^{\frac{1}{2}}M\mathbf{x}(\mathrm{t}=0)\,, \tag{D-4-4}$$

where $\mathbf{E}_{\mathrm{f}}$ is the final norm operator, $\mathbf{x}$ is the set of initial perturbations, $\mathbf{M}$ is the linear propagator of the model for optimization time period, *M* denotes time integration by the nonlinear forecast model, and (,) denotes the Euclidean inner product of two vectors. Generally, although singular vectors are ensured maximum growth in the linear model, they do not always grow very much in the nonlinear model because the tangent linear approximation occasionally becomes invalid owing to the strong nonlinearity in the forecast model. For the third and fifth singular vectors, there were obvious affinities between linear and nonlinear growth rates and patterns of initial perturbations, whereas the other singular vectors showed low correlations.

Figure D-4-1 shows the horizontal distribution of vertically integrated energy of the MSVs at both initial and final times. The areas of sensitivity of the second and third leading singular vectors were around the Bohai Sea, where a low-pressure system was observed, while the sensitive region of first singular vector lay on the west side of the low-pressure system. The final norm of the second and third singular vectors was concentrated near the region where intense precipitation was predicted by the forecast model that provided the basic fields for the TLM and ADM. This feature indicated that MSVs with a moisture norm tended to capture small-scale disturbances accompanying moderate and intense rainfall, which can be an advantage for a short-range ensemble forecast. However, the horizontal scale of the initial perturbations was very localized. Therefore, we considered that further modifications were needed, such as the use of the variance minimum method and adjustment of the amplitudes of the initial perturbations.

Figure D-4-2 shows the variation in ensemble spreads of surface variables in the MSV experiment and the WEP experiment (the downscaled JMA one-week EPS). The WEP experiment required little computational time to prepare the initial perturbations so it was regarded as a reference method. The MSV spreads were much smaller than the RMSEs of the ensemble mean, though the growth rate of the spreads was higher than in the WEP experiment. The RMSEs of the ensemble mean are presented in Fig. D-4-3. For both the sea level pressure and surface (2 m) temperature fields, the RMSEs of the ensemble mean were little different than those of the control forecasts in the MSV experiment, whereas the superiority of the ensemble means over the control forecasts is obvious in the WEP experiment.

These experiments showed some disadvantages of MSVs, such as the shortage of ensemble spreads originating from very localized initial perturbations and insufficient improvement of the ensemble mean forecast. In addition, MSV calculation required more computation time than other perturbation methods tested at MRI/JMA. These features were modified by using dry TLM and ADM models in which moist processes were ignored. However, with dry models, initial perturbations of the moisture fields could not be obtained, though they are critical for short-range ensemble predictions aimed at producing probabilistic forecasts of local severe weather, because the uncertainty of the moisture fields included in initial fields is not small owing to the inadequate observational network. To address these shortcomings, we modified the MSV method and tested the modified method in the 2008 preliminary experiment (see section E-4-3).

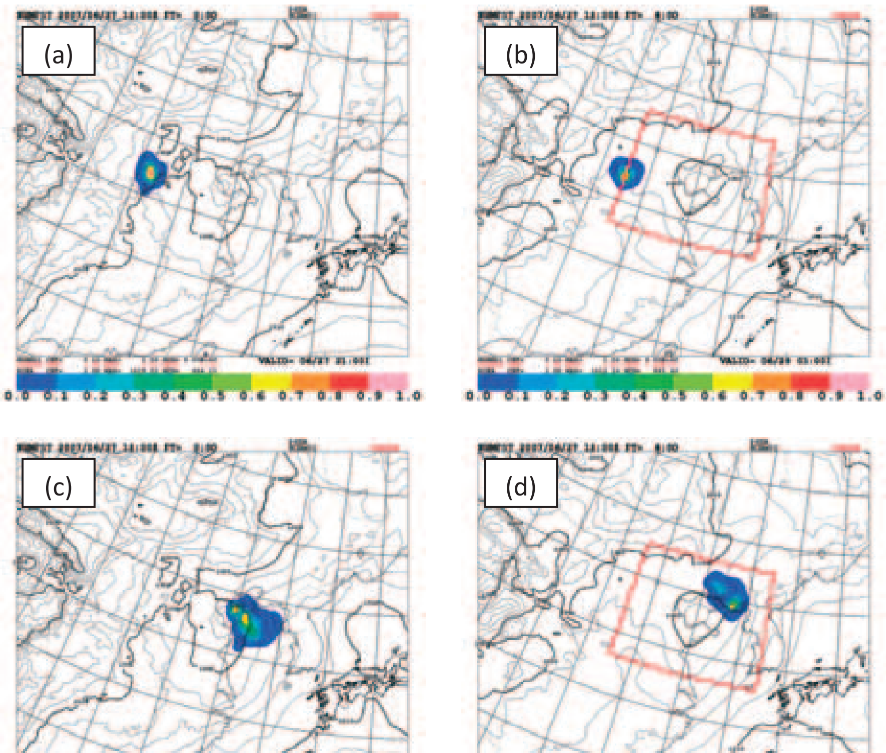

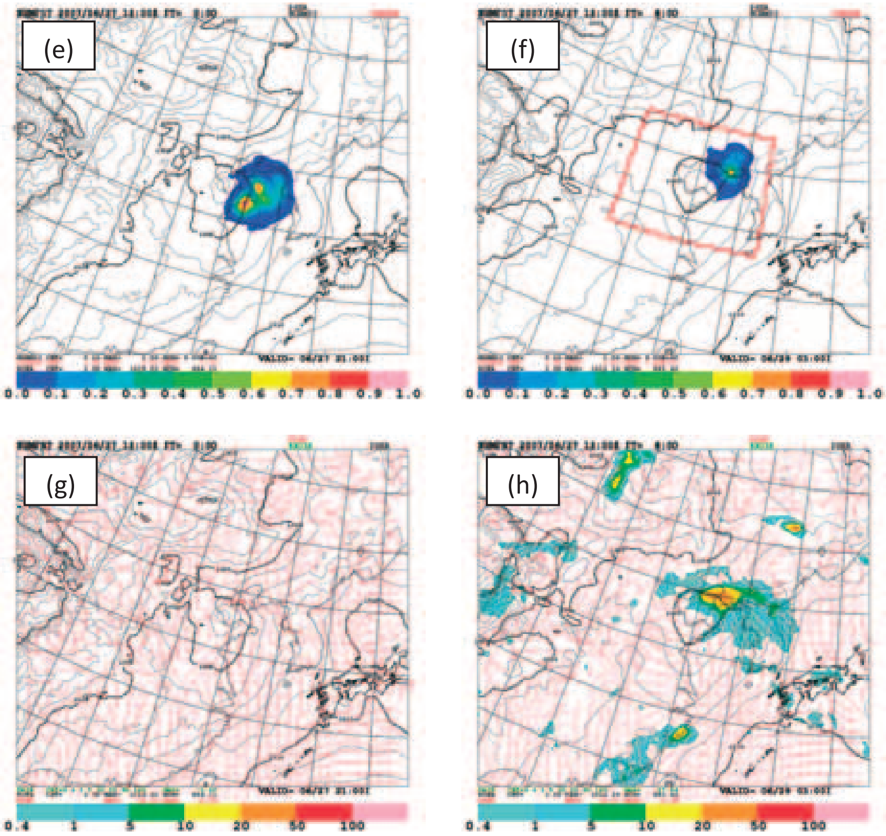

Fig. D-4-1. Horizontal distributions of vertically integrated total energy of MSVs. (a) First SV at the initial time 12 UTC on 27 June 2007; (b) first SV at the final time 00 UTC on 28 June 2007; (c) and (e) are the same as (a) but for the second and third SV, respectively; (d) and (f) are the same as (b) but for the second and third SV, respectively; (g) sea surface pressure (contours) and windfields (arrows) of the forecast (nonlinear) model at the initial time; and (h) is the same as (g) but at the final time.

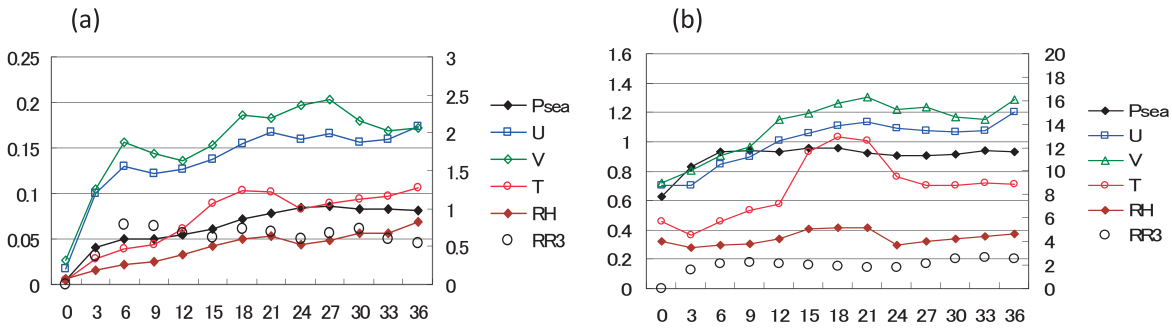

Fig. D-4-2. Variation of the ensemble spread in the experiment using (a) MSVs as initial perturbations (MSV) and (b) the JMA global EPS perturbations as initial perturbations (WEP). The experimental period was from 27 to 30 June 2007.

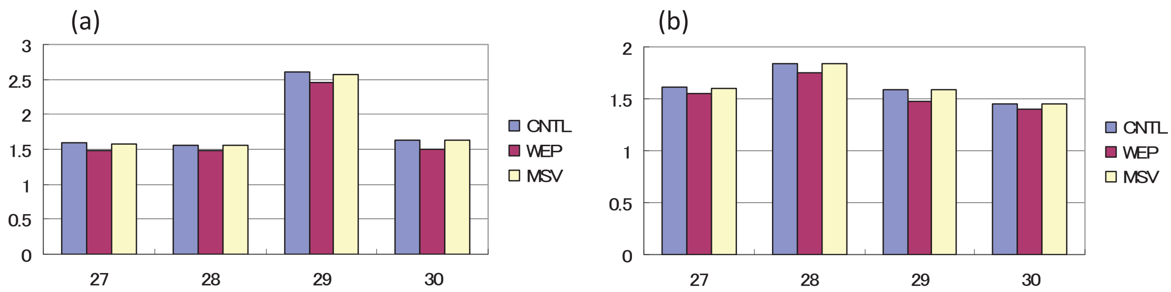

Fig. D-4-3. RMSEs (FT=24) against analysis fields. (a) Sea level pressure and (b) surface (2 m) temperature. The experimental period was from 27 to 30 June 2007.

Table D-4-1. Specification of the MSVs for the 2007 B08RDP experiment.

Specification of the Meso SV	
Horizontal mesh	117 × 101 (Δx = 30 km, Δt = 120 s), LMN
Vertical levels	40 (Δz = 40－1180 m)
Norm	Total Energy Norm (wt = 3.0, wq = 0.5)
Optimization time	6 hours
Moist physics	Large-scale condensation
Convection	Moist Convective Adjustment
Lanczos iteration	20 times (using the leading 5 SVs for ensemble prediction)
Target area	Beijing area (33.0－43.0°N, 112.5 – 127.5°E)

Table. D-4-2. Relationships among singular values (Sval), nonlinear growth (Nlg), and their similarity index (SI) for each MSV. The initial time was 12 UTC on 27 June 2007, and the optimization time was set to 6 hours.

	Sval	**Nlg**	**SI**
1	5.047	3.987	0.537
2	4.494	3.882	0.522
3	3.849	3.873	0.895
4	3.837	3.076	0.571
5	3.458	3.084	0.776

D-4-4. Mesoscale breeding growing mode (MBD) method

The breeding growing mode (BGM) method is a typical way to produce initial perturbations in the ensemble prediction. It selectively raises the Lyapunov vectors using the forecast model in the breeding cycle and has been widely used in several operational EPSs including the JMA global EPS until May 2007 and the NCEP's Short Range Ensemble Forecast (SREF) system. In the 2006 experiment, a mesoscale breeding (MBD) method which employs the self-breeding cycle with the JMA nonhydrostatic model was developed.

To evaluate the magnitude of the bred perturbations, the moist total energy norm by Barkmeijer et al. (2001):

$$TE = \frac{1}{2}\iint \{(U_P - U_C)^2 + (V_P - V_C)^2\} + \{\frac{c_p}{\Theta}(\theta_P - \theta_C)^2\} + w_q \frac{L^2}{c_p\Theta}(q_P - q_C)^2 dSdP$$

$$+\frac{1}{2}\int \{\frac{R\Theta}{P_r}(P_{seaP} - P_{seaC})^2\}dS, \qquad \text{(D-4-5)}$$

was employed. Here, according to the JMA global EPS, the values of Θ =300 K, P_r = 800 hPa and w_q=0.1 were used and the norm was computed less than 5.3 km above ground level (AGL) height.

As shown in Fig. D-4-4, 12 hourly self breeding cycles with a horizontal resolution of 15 km were conducted twice (24 hours). Perturbations from the operational global one week EPS of one day before were used as the initial seed of ensemble perturbation. The moist total energy norms are computed by the differences between the control runs and perturbed runs, and the bred perturbations of all prognostic variables except soil temperatures are normalized every 12 hour. The normalization coefficients are determined by the square root of ratios between the total energy norms of perturbed runs and a standard norm, which is computed by prescribed values of model variables (0.35 hPa for MSL pressure, 1.0 m/s for U and V, 0.4 K for θ and 5 % for relative humidity, respectively). These values are about 50 % of the magnitudes of JMA's operational Meso 4DVAR's (Koizumi et al., 2005) statistical background errors.

Five bred vectors were added to and subtracted from the initial condition of the control run (initial condition of RSM produced from the regional 4D-Var analysis of JMA) to make five positive and negative ensemble members, i.e., totally 10 ensemble members.

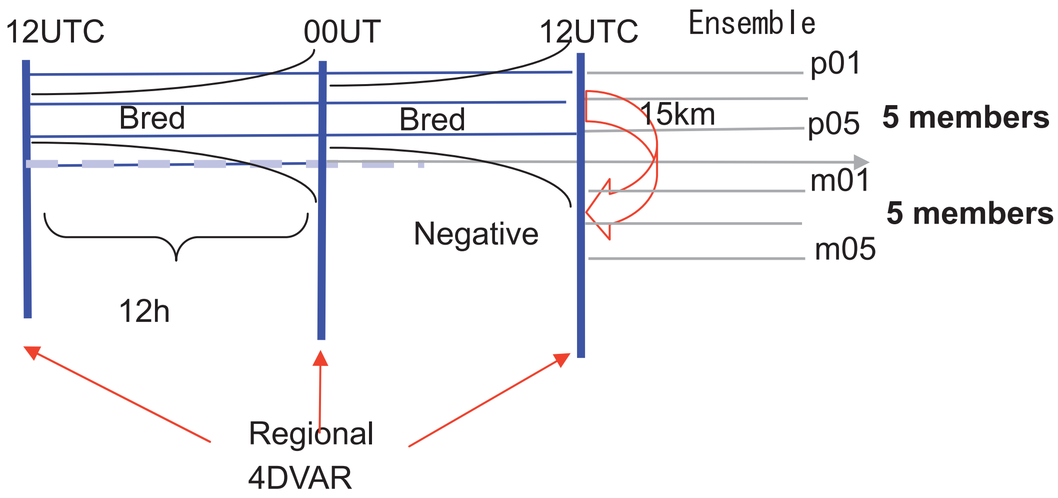

Fig. D-4-4. Schematic chart of the MBD method in the 2007 experiment.

D-4-5. Comparison of four methods

Prior to the 2007 preliminary experiment, performances of the previously mentioned four initial perturbation methods were compared by verifying the ensemble spreads and RMSEs of the ensemble mean.

a) Comparison of MSV and WEP

Comparison of the MSV method and the WEP method were made for 4 days from 27 to 30 June 2007. Figure D-4-5 compares ensemble spreads of MSV and WEP at various forecast times (FT). The initial growth rate of ensemble spreads in the MSV method is large up to FT=6, however, as seen in the unit of the ordinate, the amplitudes of spreads in the MSV method were very small. Figure D-4-6 compares RMSEs of mean sea level pressure and surface temperatures at FT=24 against the initial condition. RMSEs by WEP are smaller than those by the control run, but in MSV, the improvement is smaller than WEP. This little improvement of RMSE in the MSV method was mainly caused by the underestimation of ensemble spread.

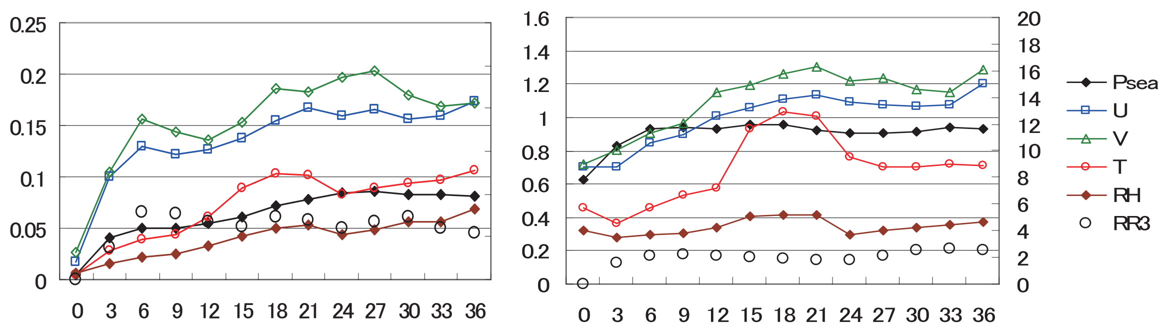

Fig. D-4-5. Time sequence of ensemble spreads for surface conditions (PSEA; sea level pressure, U and V; 10m winds, T; 2m temperature, R3; 3 hour accumulated rain, RH; 2m relative humidity). Unit on the vertical axis is hPa for PSEA, m/s for U and V, degree for T, mm for R3 and % for RH. Verification period is 4 days from 27 to 30 June 2007. Left) MSV. Right) WEP.

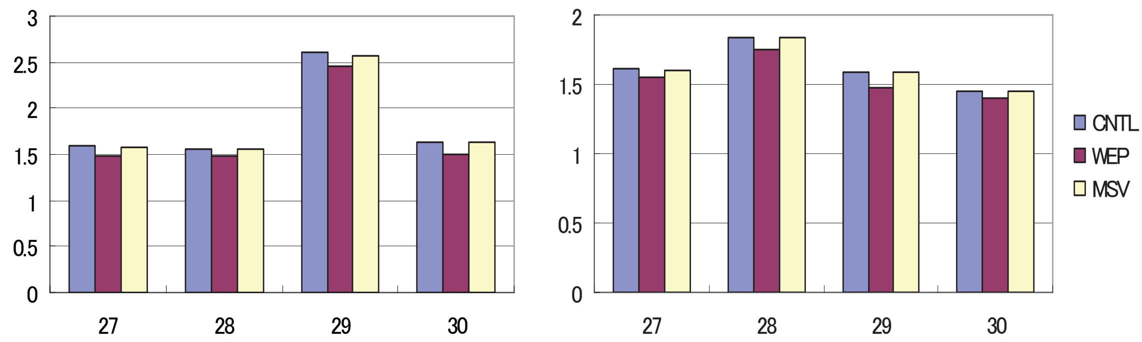

Fig. D-4-6. RMSEs of mean sea level pressure at FT=24 against the initial condition. Left) Mean sea level pressure. Right) surface (2m) temperatures.

b) Comparison of MBD and WEP

Similar comparisons were made for MBD and WEP methods for 2 days from 10 to 11 July 2007. In the case of MBD, the amplitude of initial ensemble spreads was comparable to that of WEP, but it did not increase with time (Fig. D-4-7). As shown in Fig. D-4-8, improvements of RMSEs were also insufficient in MBD compared with WEP.

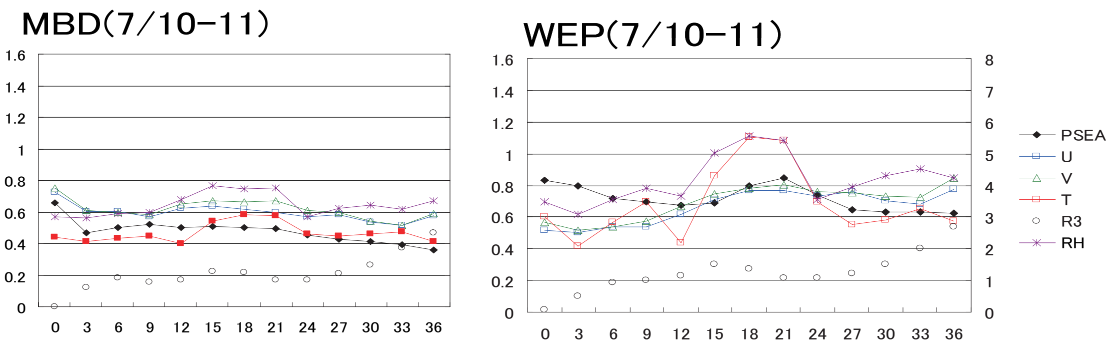

Fig. D-4-7. Same as in Fig. D-4-5, but for comparison of MBD (left) and WEP (right). Verification period is 2 days from 10 to 11 July 2007.

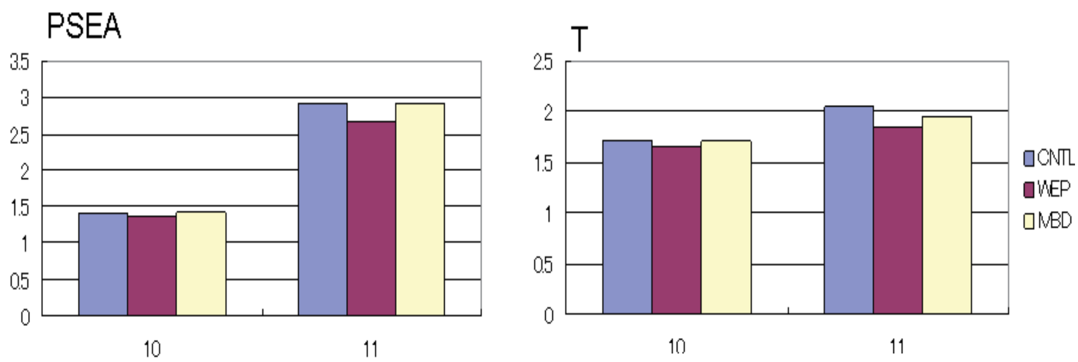

Fig. D-4-8. Same as in Fig. D-4-6, but for comparison of MBD and WEP.

c) Comparison of GSV and WEP

Comparisons between GSV and WEP methods for 5 days from 2 to 6 July 2007 are shown in Figs. D-4-9 and D-4-10. In the case of GSV, the amplitude of initial ensemble spreads was smaller than WEP, while it increased with time and became larger after FT=24 (Fig. D-4-9). As shown in Fig. D-4-10, RMSEs of the GSV method were also smaller than those of WEP method.

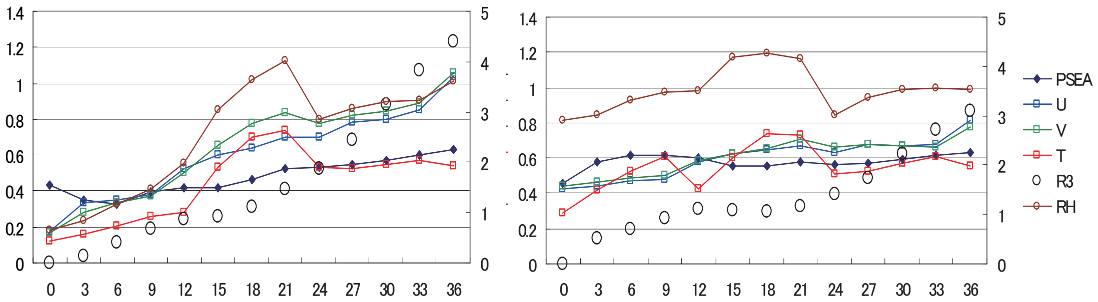

Fig. D-4-9. Same as in Fig. D-4-5, but for comparison of GSV (left) and WEP (right). Verification period is 5 days from 2 to 6 July 2007.

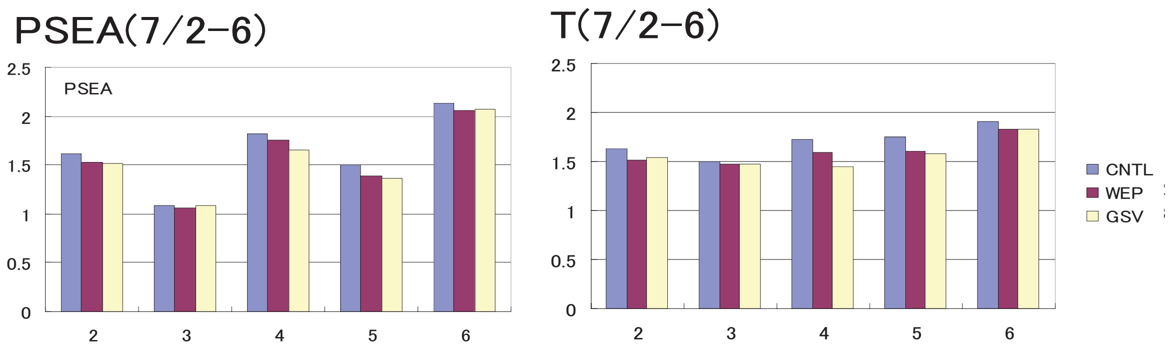

Fig. D-4-10. Same as in Fig. D-4-3, but for comparison of GSV and WEP.

In the above comparisons, only the GSV method outperformed WEP, the downscale of operational global EPS perturbations. Considering the above performance of four methods, GSV was adopted as the initial perturbation method in the 2007 experiment.

D-5. Perturbation for soil temperature

In the 2006 experiment, we found that the screen temperature at the height of 2m (T2m) was not predicted properly, when the performance of the ensemble forecasts of JMA/MRI was checked by comparing with the observed temperatures. Figure C-6-1 is the Talagrand diagram of T2m, which is diagnosed from the temperatures of ground surface (Tsurf), i.e. the most upper soil layer, and of the lowest layer of atmosphere (T20m) using the Monin-Obkhov similarity. This diagram indicates that most of the observed temperatures were distributed outside of the range of T2m obtained by the ensemble forecasts. Namely, the spread of T2m were underestimated compared with the observed temperatures.

In the 2006 experiment of JMA/MRI, no perturbation was added to the initial soil temperature that was predicted explicitly. Because the soil temperature influences T20m, then the spread of T20m must be small. As mentioned before, T2m was produced from Tsurf and T20m. Thus, it is deduced that the non-perturbed soil temperature is one of the reasons of the small spread of T2m. To enlarge the spread of T2m, the soil temperature was perturbed according to the relation between the soil temperatures and T20m.

In the NHM used in this project, soil temperature was composed of 4 layers (Tsurf, Tin2 and Tin3 and Tin4), and the soil temperature of lowest soil layer (Tin4) was set to be the climatological value. Figure D-5-1 is the scatter diagrams of relative temperatures against Tin4. This scatter diagram was obtained from 24h-forecast of CNTL from 8 to 11 July 2007. CNTL is the experiment of which initial condition was produced without adding any perturbations. The horizontal axes in Fig. D-5-1, which are common in three diagrams, are the relative temperatures of T20m against Tin4, i.e., T20m-Tin4. The vertical axes are the relative temperatures from the first to third soil layers against Tin4, i.e., Tsurf-Tin4, Tin2-Tin4 and Tin3-Tin4. We assume that 24 hour is enough for the soil temperature (Tsurf, Tin2 and Tin3) to follow T20m.

The scatter diagrams indicate that Tsurf-Tin4, Tin2-Tin4 and Tin3-Tin4 were well correlated with T20m-Tin4. Especially in the relation of the most upper soil layer (Tsurf-Tin4 vs T20m-Tin4), the slope of the relation was close to 1 and bias is only 0.2 degree. As for the layers in the ground, Tsurf-Tin4, Tin2-Tin4 and Tin3-Tin4 were well correlated to T20m-Tin4, though their slopes against T20m-Tin4 were smaller and their biases became larger. Therefore, soil temperatures were produced using these relations from T20m-Tin4.

Figure D-5-2 shows the temporal variations of the ensemble spreads without and with perturbation of soil temperatures. When the soil temperature was perturbed, the spread of surface temperature is slightly increased. However, the improvement of the initial soil temperature could maintain only for 12 hours, as indicated by red arrows in Fig. D-5-2. In general, the perturbations of atmosphere at the lower layers that was produced by SV methods are relatively small. Therefore, the processes that determine the soil temperature, such as insolation, overcome the impact of the initial perturbation of soil temperature after the forecast time of 12 hour. The method that perturbs the soil temperature should be ameliorated.

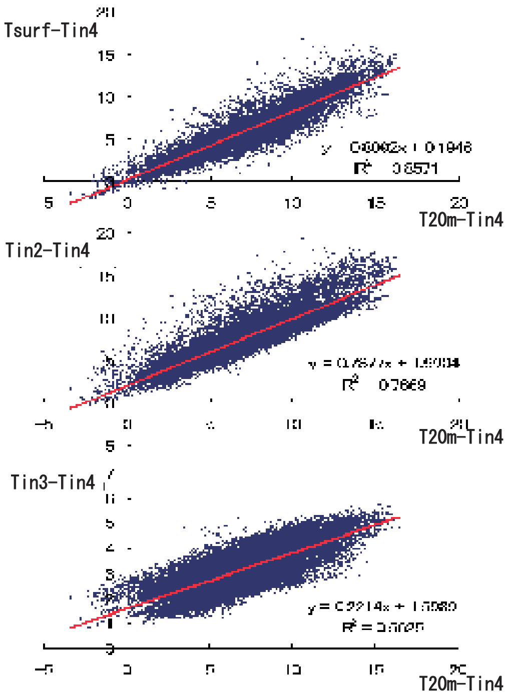

Fig. D-5-1. Scatter diagrams of the relative temperatures of Tsurf, Tin2, Tin3 and T20m against Tin4. Scatter diagrams were obtained from the 24-h forecast of CNTL from 8 to 11 July 2007.

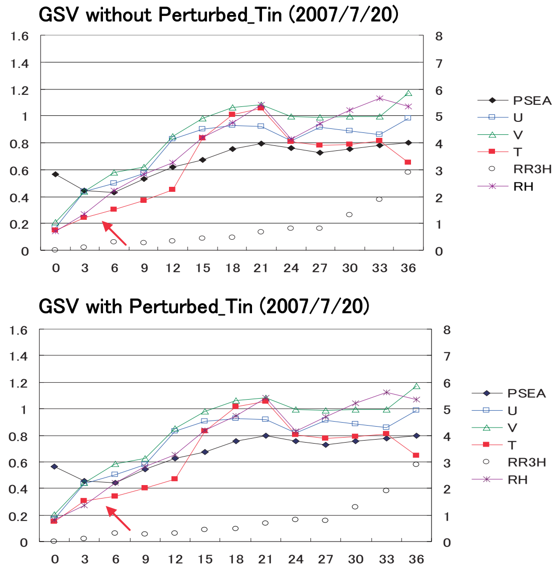

Fig. D-5-2. Time sequence of spreads of T2m with and without the perturbation of soil temperature. Spread of T2m was slightly increased when the soil temperatures were perturbed, though their effect is not large.

D-6. Experimental system

D-6-1. Experimental system

Experimental system of MRI/JMA used in the 2006 preliminary experiment was designed to use only WEP, downscaling of initial perturbations derived from the JMA weekly global EPS, for initial perturbation method. Moreover, we couldn't easily control the individual jobs composing the system. In the 2007 experiment, to verify performances of other initial perturbation methods, such as GSV, MSV and MBD, we reconstructed the experiment system of ensemble forecasting revising the system more flexible for the future development. Motivated by these backgrounds, we performed the modification of the system extensively.

The system used in the 2007 experiment consisted of seven job steps, which are listed in Table D-6-1.

(i) PREMF: Running a 12-hour control forecast used in subsequent MKPTB process (only MBD method).

(ii) MKANAL: Preparation of analysis fields used as initial conditions in the following job MKGRD. We could select either of the JMA operational regional analysis (RA) or the JMA Meso 4D-Var analysis over Beijing area (MA). When RA was selected, we could utilize the operational analysis without any further work because the data had been sent from the JMA to MRI in a delay of a few hours. By contrast, because the operational Meso 4D-Var analysis didn't cover the forecast domain for B08RDP fully, we carried out the Meso 4D-Var analysis improved for this experiment when MA was selected (see E-3-1). This procedure needed about 2 hours for our computer resources, which could be rather weighty for quasi-real time operation in B08RDP.

(iii) MKGRD: Preparation of input data files utilized in a model forecast, such as initial and lateral boundary conditions, topography, SST and parameter on the earth's surface. Either of the initial conditions MA and RA was used as no-perturbed initial condition in ensemble forecasting.

(iv) MF: Performance of a control forecast. This job could be unified the following job MEP, treated as one member of ensemble forecasts.

(v) MKPTB: Generation of initial perturbations by either of four methods, WEP, GSV, MSV and MBD. Computation times required in individual methods were considerably different. MSV, the most costly system of them, needed about 80 minutes whereas WEP and MBD methods needed only 11 minutes at most.

(vi) MEP: Performance of ensemble forecasts with parallel execution of every 4 member.

(vii) POST: Data deformation and transmission. Forecast data needed to be transferred to the CMA server after interpolated to a resolution of 0.15° latitude and longitude in grib2 format. In addition, specific elements such as CAPE, CIN, SAUI (D-6-3, E-6-3) were required to be sent.

In this system, we were able to execute optional jobs selectively without going through all of the processes. This feature of the system was suitable for research experiment, especially for its developing stage. As for the initial condition, we planned to use MA at first. However, we found some bugs in the treatment of surface temperature in MA, we finally used RA for initial condition of the control forecast.

All ensemble forecast data were interpolated and encoded in grib2 format in the POST process before they were transferred to CMA. For detail, see D-6-3.

Table D-6-1. Job list of ensemble forecasting system of MRI/JMA in 2007.

Job Name	Function
PREMF	Pre-processes for the breeding method
MKANAL	Preparation of initial conditions for the control run
MKGRD	Making initial and boundary files
MF	Running the control run (optional)
MKPTB	Generation of initial perturbations by WEP, GSV, MSV and MBD methods.
MEP	Ensemble forecasting
POST	Post-processes

D-6-2. Web visualization

To monitor the results of ensemble forecasts with internal web pages, the figures of ensemble mean, spread and stamp map of each ensemble member were produced in the operational procedures at MRI/JMA. The figures for the web page were plotted with the graphic software of 'GrADS' (http://grads.iges.org/grads/). The outputs of the ensemble forecast were the data with the horizontal grid interval of with 15 km in the JMA original format (NuSDAS), while data that the CMA requested was in latitude and longitude coordinated format. First, the data with the horizontal grid interval of 15 km was converted to that in latitude and longitude coordinated format by the program of 'mapconv', of which original version was produced by Tabito Hara of JMA. Because the additional data (Convective Available Potential Energy etc.) of ensemble forecasts were requested by the CMA, the calculation of these parameter distributions was also conducted in 'mapconv'. The outputs of ‘mapconv’ remained in NuSDAS format. Then data in 'GrADS' format were produced from the outputs of 'mapconv' by the program of ‘nus2grd’. The figures that were plotted from the output of ‘nus2grd’ with 'GrADS' software were uploaded automatically to the MRI data server so that the results of ensemble forecasts can be checked by the collaborators of JMA headquarters and other participants of the project. The web page for figures of the ensemble forecasts had a simple structure. Namely, figures were displayed as catalog of figures with indexes of date, variables and so on (Figs. D-6-1, D-6-2 D-6-3 and D-6-4). Similar web-visualization was also conducted in the 2006 experiment.

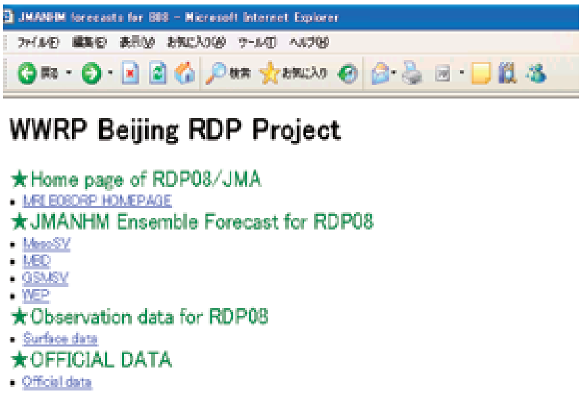

Fig. D-6-1. Main menu of the web page for B08RDP experiment. The ensemble forecasts of 4 initial perturbation methods, CMA's observation data and the final ensemble forecasts of MRI/JMA were included in the items of the menu.

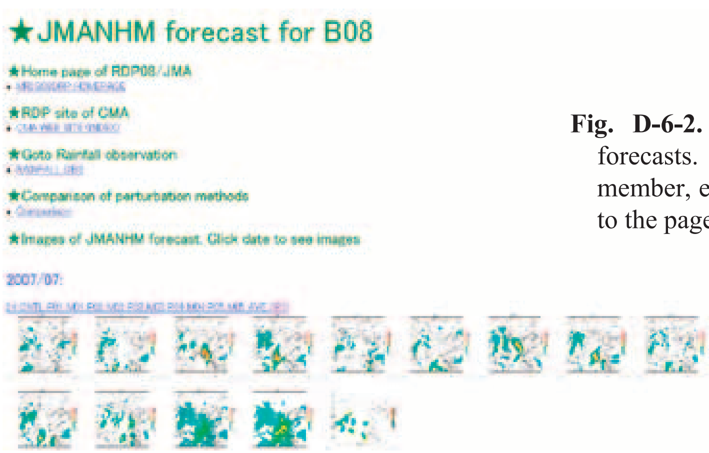

Fig. D-6-2. Menu of final results of ensemble forecasts. Clicking the names of ensemble member, ensemble mean and spread, we can jump to the page of the selected titles.

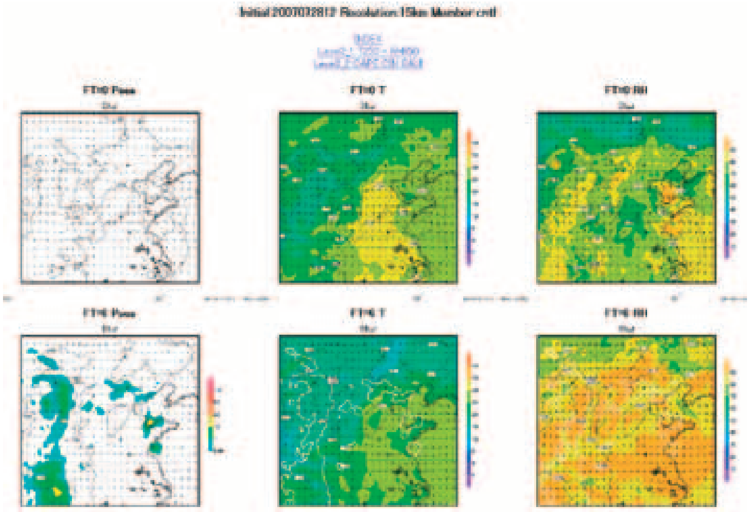

Fig. D-6-3. Example of a web page for each ensemble member. Figures of FT=0-36 hour were automatically plotted with the interval of 3-hour in the operational procedure of the experiment. The figures, of which data were requested by the CMA, can be selected by items under the main title.

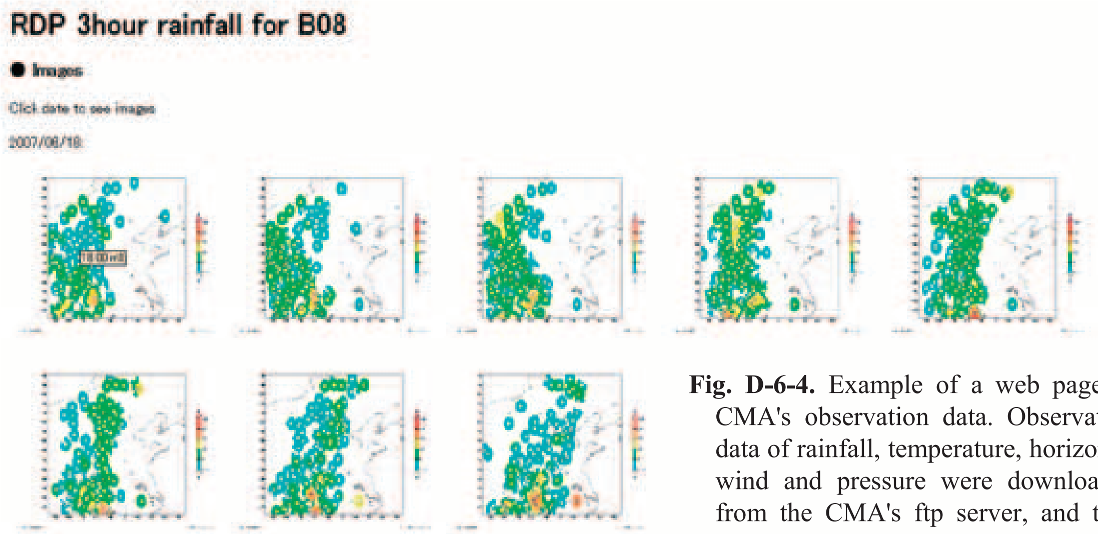

Fig. D-6-4. Example of a web page of CMA's observation data. Observation data of rainfall, temperature, horizontal wind and pressure were downloaded from the CMA's ftp server, and then their distributions were plotted automatically.

D-6-3. GRIB-2 transformation

Because the CMA requested the ensemble forecast data in grib2 format, which is the format of TIGGE LAM, the conversion from the ensemble forecast in JMA original format (NuSDAS) to the data in grib2 format was performed by the tool of 'nus2grib2'. The converted data were checked by figures and logs produced by the tool of 'grib2viewer' (Fig. D-6-5).

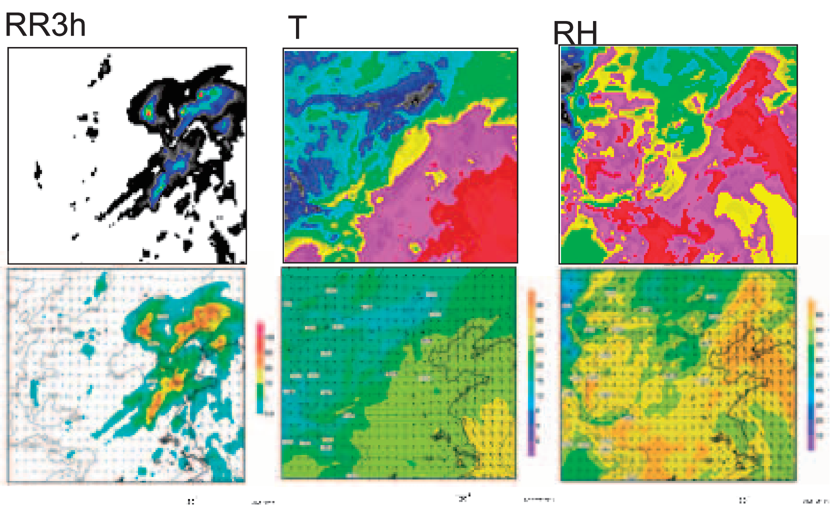

Fig. D-6-5. Horizontal distributions of 3-hour rainfall amount (RR3h), surface temperature (T) and relative humidity (RH) at the height of 2 m. Upper and lower panels are the outputs of 'grib2viewer' and 'GrADS', respectively.

D-7. Verification

D-7-1. Verification tests performed by the MRI

The participating centers in the 2007 preliminary experiment and their ensemble forecast specifications are listed in Table D-1-1. In the preliminary experiment of 2007, the Austrian Zentral Anstalt fur Meterologie und Geodynamik and Meteo-France, referred to here as ZAMG, sent jointly acquired ensemble forecast results to CMA. Most participating centers sent mesoscale ensemble forecast results, but NCEP sent global ensemble forecast results. One objective of our RDP project was to demonstrate the merits of mesoscale ensemble forecasts. Thus, the NCEP data were used as reference data to demonstrate the usefulness of mesoscale ensemble forecasts.

Figure D-7-1 presents examples of the ensemble forecasts. The probabilities of 3-hour rainfall over 1 mm and the radar reflectivity distributions were obtained from the RDP and CMA websites. At 15 UTC on 10 August 2007, a rainfall band along the Shandong Peninsula was observed by CMA operational radars (Fig. D-7-1a). The models of most participants predicted this rainfall band well. One day before the passage of this rainfall band through the Shandong Peninsula, scattered weak rainfall occurred near Beijing (Fig. D-7-1b). However, the distributions of this rainfall predicted by the ensemble forecasts of the participating centers were varied. Namely, the MRI/JMA, MSC, and ZAMG ensemble forecasts showed rainfall occurring near Beijing, whereas those of CMA and CAMS showed a region of rainfall in a wider area around Beijing. The performance of the ensemble forecasts thus depended on both the specific weather conditions and the participating center.

Because useful information can be obtained by comparing results among the participants, MRI downloaded the ensemble forecast data of the other participating centers from the CMA data server, and then calculated their bias scores and threat scores. Figure D-7-2 shows the bias and threat scores for surface temperature (T2m), based on a verification period covering the 11 days from 26 July to 5 August 2007. Compared with the forecasts of other participating centers, the MRI/JMA bias score for temperatures exceeding 35 °C was relatively small. The low score for 37.5 °C indicates that the

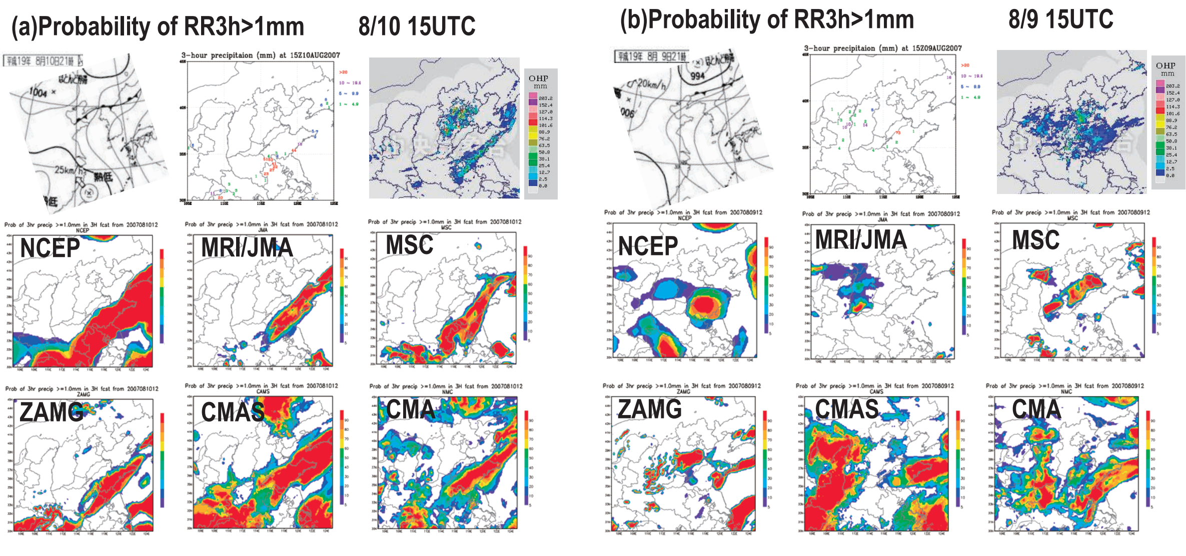

Fig. D-7-1. Example ensemble forecasts of the participating centers. Three-hour rainfall data, the figures of reflectivity, and of the probability of 3-hour rainfall exceeding 1 mm were obtained from the RDP and CMA web sites. The distributions shown are from 15 UTC on (a) 10 August and (b) 9 August.

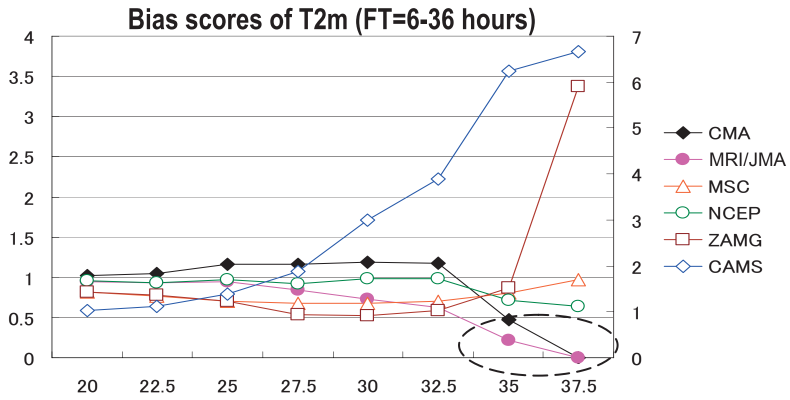

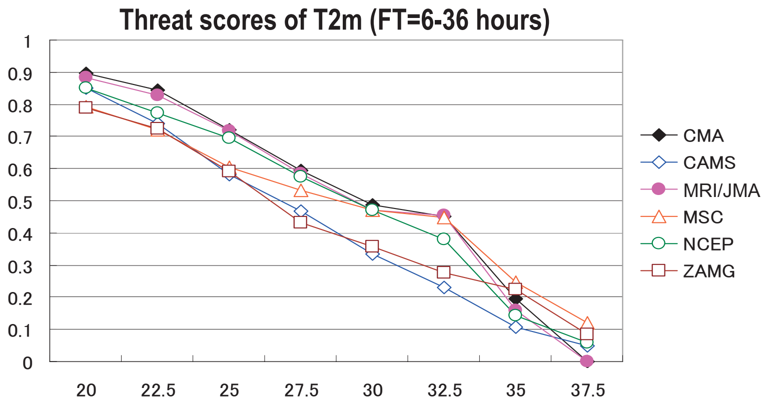

Fig. D-7-2. Bias and threat scores for surface temperature (T2m). The score verification period was the 11 days from 26 July to 5 August 2007. FT is forecast time.

daytime temperature reproduced by MRI/JMA's ensemble forecasts rarely exceeded 35 °C even though the observed temperature often exceeded 35 °C. To overcome this problem, the treatment of soil wetness was revised in the 2008 experiment (see E-2-2).

We also compared the 6-hour rainfall (RR6h) scores for the same verification period (Fig. D-7-3). The MRI/JMA bias scores for 6-hour rainfalls of less than 10 mm were smaller than those of the other participating centers. The MRI/JMA equitable threat scores, however, were better than those of the other participating centers, with the exception of those for 6-hour rainfalls from 3 to 5 mm. These results suggest that MRI/JMA underestimated rainfalls of less than 10 mm. To overcome these problems, the Kain-Fritsch parameterization and some cloud microphysical parameters were fine-tuned in the 2008 experiment (see sections E-2-1 and E-2-3).

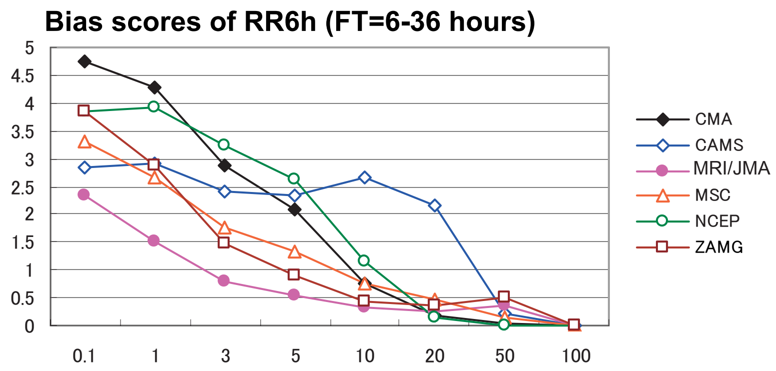

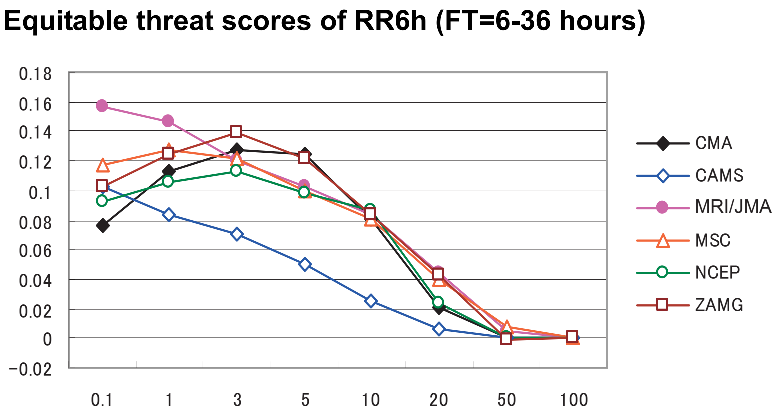

Fig. D-7-3. Bias and threat scores for 6-hour rainfall (RR6h) during the verification period, 26 July to 5 August 2007.

D-7-2. Verification by CMA

Verification of the 2007 experiment was performed by CMA and presented at the third B08FDP/RDP workshop (Li, Y., 2007). Forecast results in the common domain (105~125°E, 30~45°N) were interpolated to verification grids with a resolution of 0.15° and compared with 400 synoptic observation stations and 722 dense auto observation stations as in the 2006 experiment. In 2007, upper air variables were also verified with 28 radio sonde stations (Fig. D-7-4).

Figure D-7-5 shows the ensemble spread and RMSE of the MRI's EPS for temperatures at 250, 500 and 850 hPa levels. The spread and RMSE of temperatures in all three levels grows gradually with the forecast time, but spreads are smaller than forecast errors. Magnitudes of RMSE were relatively smaller than that of other participants (figures not shown).

Figures D-7-6 and D-7-7 show the ensemble spread and RMSE of 500 hPa height field and relative humidity at 850 hPa level. Magnitudes of ensemble spreads against forecast errors were about 60 % at FT=24.

Talagrand diagrams for surface and 850 hPa temperatures and wind speeds are given in Figs. D-7-8 and D-7-9. As in the 2006 experiment, spread of surface temperature forecast was smaller than observation, and suggested underestimation of high temperature. Histogram for 850 hPa wind was relatively flat.

Similar tendencies were found in other participants' results. RMSE of surface temperature and relative humidity of the ensemble mean of MRI/JMA EPS were relatively small compared with other participants (figure not shown).

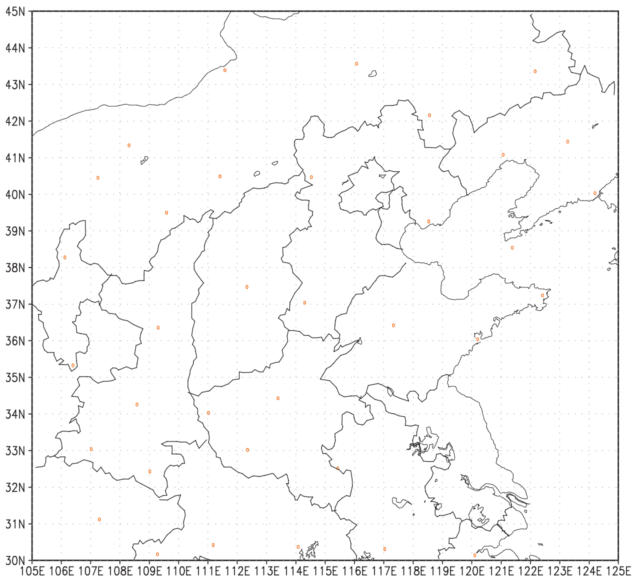

Fig. D-7-4. Radio sonde observation points used for verification in B08 RDP. After Li Y. (2007). Courtesy of NMC/CMA.

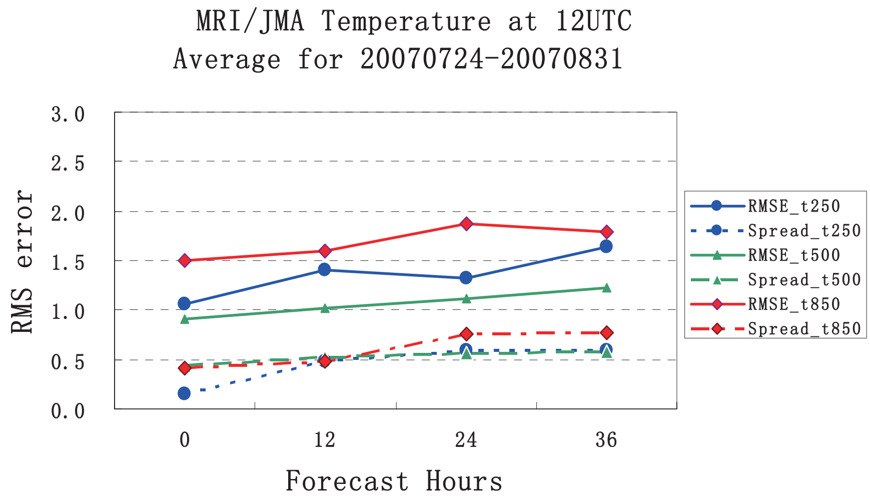

Fig. D-7-5. Ensemble spread and RMSE of temperatures by MRI EPS at 250, 500 and 850 hPa levels. Period is 39 days from 24 July to 31 August 2007. After Li Y. (2007). Courtesy of NMC/CMA.

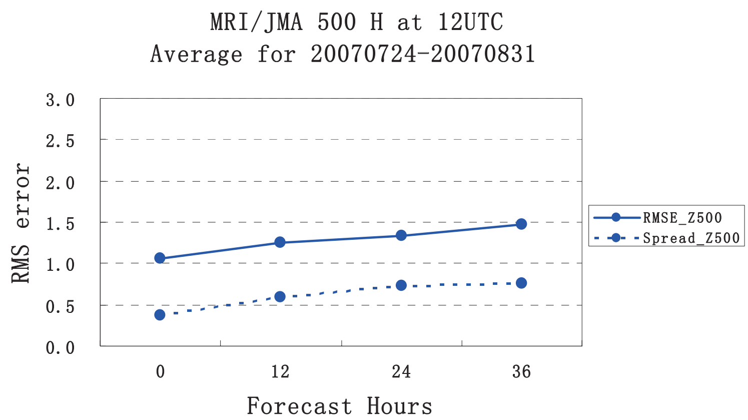

Fig. D-7-6. Same as in Fig. D-7-5, but for 500 hPa height. Unit of vertical axis is 10 m. After Li Y. (2007). Courtesy of NMC/CMA.

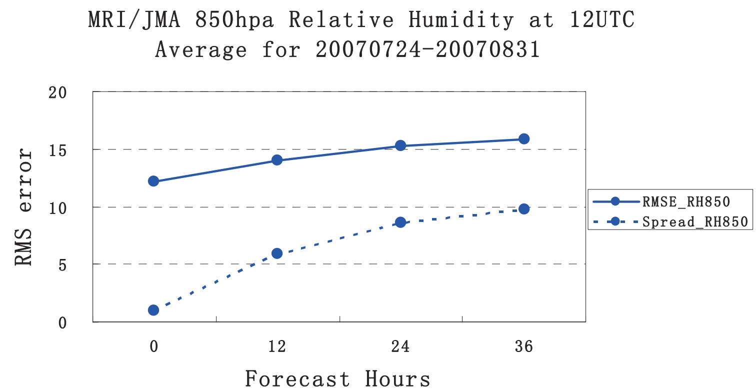

Fig. D-7-7. Same as in Fig. D-7-2, but for 850 hPa relative humidity. After Li Y. (2007). Courtesy of NMC/CMA.

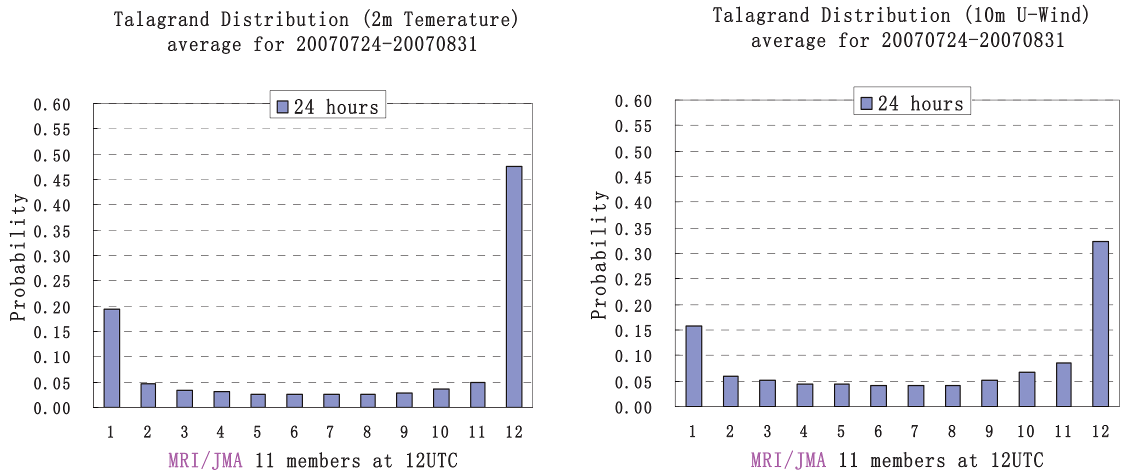

Fig. D-7-8. Talagrand diagram on surface (2m) temperature (left) and 10m wind speed (right) at FT=24 of the MRI/JMA ensemble forecast. Period is 39 days from 24 July to 31 August 2007. After Li Y. (2007). Courtesy of NMC/CMA.

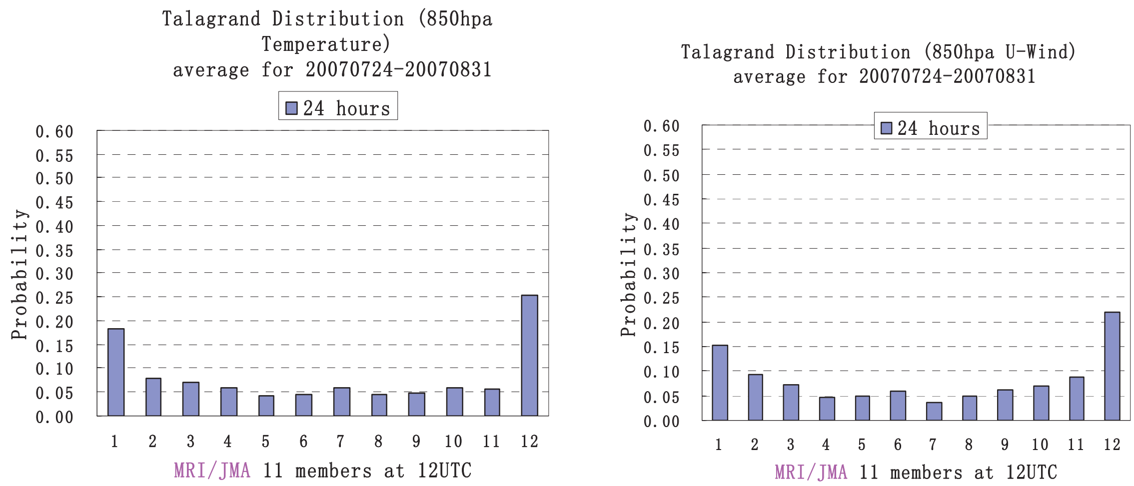

Fig. D-7-9. Same as in Fig. D-7-5 but for temperature (left) and wind speed (right) at 850 hPa level. After Li Y. (2007). Courtesy of NMC/CMA.

Relative Operation Characteristic (ROC) curve for weak rain (0.1 mm/6 hours) verified by CMA is shown in Fig. D-7-10. False alarm rate for FT=12 is less than 20 %, which is the minimum in the six participants, while the hit rate (detection ratio) was less than 70 %, and is relatively small among the participants. This result suggests that MRI/JMA EPS tends to predict less precipitation. Figure D-7-11 shows reliability diagram. For weak rain (Left; 0.1 mm/6hours) predicted probability was close to the perfect line, but reliability for moderate rain (2mm/6hours) was insufficient.

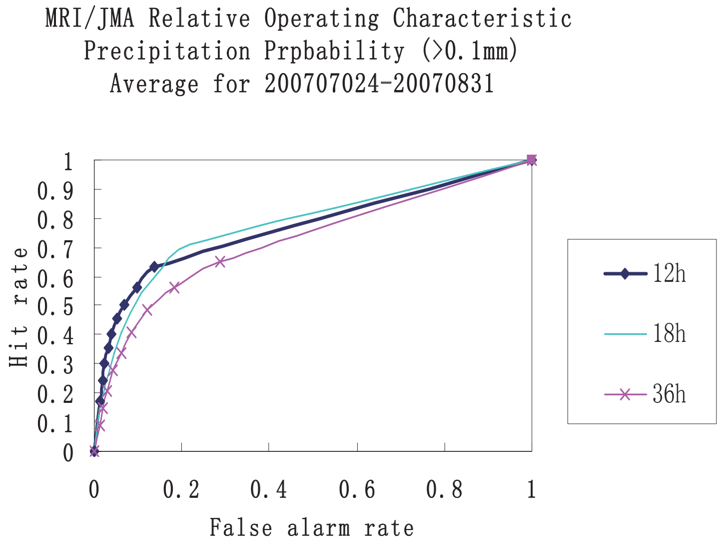

Fig. D-7-10. ROC curve for weak rain (0.1 mm/6 hours). After Li Y. (2007). Courtesy of NMC/CMA.

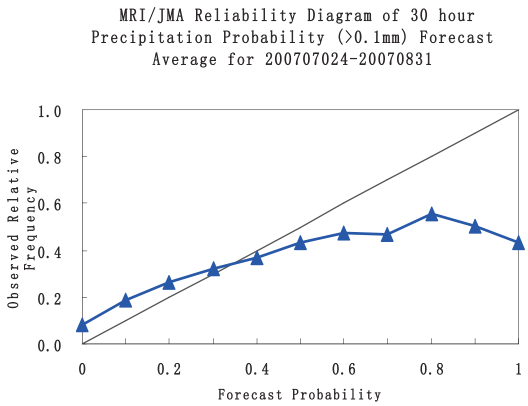

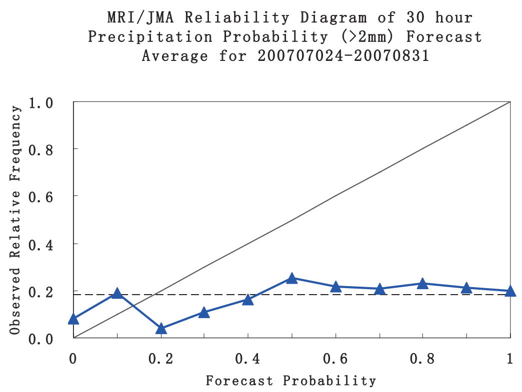

Fig. D-7-11. Reliability diagram for precipitation. Left) 0.1 mm/6 hours, Right) 2 mm/6 hours. After Li Y. (2007). Courtesy of NMC/CMA.

D-8. Tier 2 experiment

As a part of the WWRP Beijing 2008 Forecast Demonstration Project/Research and Development Project (B08FDP/RDP), in addition to the mesoscale ensemble forecasts using a 15-km grid interval (Tier 1 experiment), forecasts made with cloud-resolving models with a horizontal grid interval of 2–3 km, referred to as the Tier 2 experiment, were also performed. Targets of the Tier 2 experiment were severe weather phenomena in the Beijing area. At the second B08FDP/RDP meeting, a squall line observed in the Beijing area on 1 August 2006 was proposed as a target by a FDP participant because it is likely to be easy to reproduce by numerical modeling. Besides this squall line, a thunderstorm observed on 30 July 2007 was proposed as another target at the third B08FDP/RDP meeting.

Downscale experiments of these two events were conducted with a non-hydrostatic model (NHM) with the horizontal resolution set to 3 km, so that the domain covered a 600 km × 600 km around Beijing. The initial and boundary conditions were produced by horizontal and temporal interpolation of the Tier 1 ensemble outputs. In the Tier 1 experiments, the JMA operational regional 4D-Var analysis data were used for the initial conditions in the control run, and the normalized perturbations from the JMA one-week global ensemble prediction system (EPS) were applied to in the 10 perturbed runs.

a) Downscale experiment of squall line on 1 August 2006

Figure D-8-1c shows the reflectivity distribution observed by Beijing radar at 0904 UTC (1704 LST) on 1 August 2006. The squall line organized from thunderstorms in the mountainous region northwest of Beijing, moved southward, and then, after passing through the Beijing area, began to decay. Figure D-8-1a shows a gestational meteorological satellite (GMS) image at 09 UTC on the same day. The cloud region that developed into the squall line is indicated by a white arrow. On the southern side of this cloud region, the cloud band of a stationary front is seen extending from southern to northeastern China. Because the squall line was on the northwestern side of this stationary front, that is, on the cold-air side of the front, the atmospheric conditions where squall line developed was stable (e.g., Convective Available Potential Energy at Beijing at 00 UTC on 1 August 2006 was 0 J/kg). Because the clouds that developed into the squall line were generated in the mountainous area during the day, solar insolation and mid-level cold air probably induced the thunderstorm development in this mountainous region. Because of the stable atmospheric conditions, all Tier 1 forecasts of MRI reproduced only a region of weak rainfall on the northwestern side

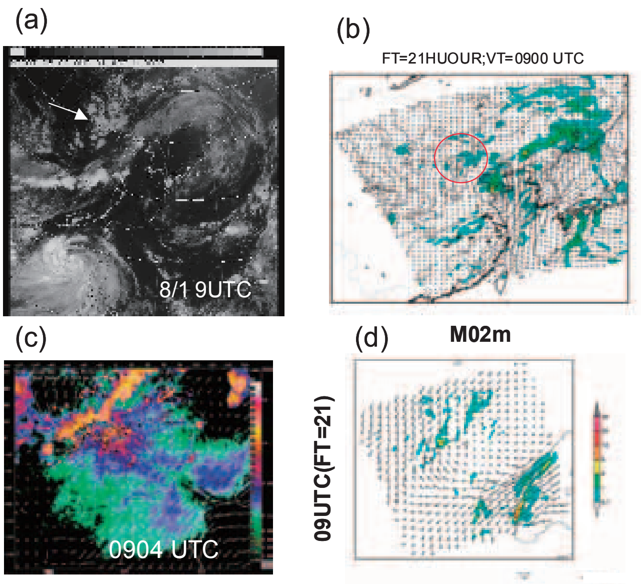

Fig. D-8-1. (a) Infra-red GMS image at 09 UTC on 1 August 2006. (b) One-hour rainfall amount reproduced by the Tier 1 ensemble experiment. (c) Reflectivity distribution at 0904 UTC, provided by Dr. Juanzhen Sun of NCAR. (d) One-hour rainfall amount simulated with a 3-km NHM.

of the stationary front (Fig. D-8-1b). This rainfall system was not organized into a squall line in the downscale experiment even when a horizontal grid interval of 3 km was used (Fig. D-8-1d). This result suggests that assimilation of mesoscale data such as Doppler radar velocity or GPS-derived precipitable water vapor (PWV) is needed to reproduce this squall line.

At the third of B08FDP/RDP meeting, Kuo et al. (2007) of NCAR presented assimilation results of ground-based GPS data, which was obtained in collaboration with the Beijing Meteorological Bureau, by using the WRF and MM5 models. They reported that they could not reproduce the squall line without assimilation of ground-based GPS data.

b) Downscale experiment of the thunderstorm on 30 July 2007

The second Tier 2 experiment target was a thunderstorm that caused 3-hour precipitation of more than 70 mm near Beijing (Fig. D-8-2a). The thunderstorm was generated west of Beijing on 29 July 2007, and subsequently moved eastward. Radar reflectivity showed an intense line shaped band extending from south to north within a region of weak rainfall (Fig. D-8-2b). This intense rain band roughly maintained its shape as it passed the Beijing area.

When ensemble forecasts were performed in the same way as in the Tier 1 experiment, the rainfall amounts and structures of the rainfall systems varied according to environmental conditions, which were modified by ensemble perturbation. In this subsection, the rainfall amounts and the structures are explained by showing the strongest (M05m) and weakest (M02p) rainfalls among the members in comparison with the control run (M00) results (Fig. D-8-3).

The line shaped band was reproduced by M05m and CNTL. The line shaped band was maintained by the convergence of a low-level southerly inflow and a cold pool. Convective cells were generated at the southern tip of the band, and then the cells moved northward with the southerly airflow above the height of 3 km. The generation point and the movement of the convective cells are key factors that determine the shape of a rainfall system. Compared with CNTL, the equivalent potential temperature (θe) of the low-level southerly inflow was higher in M05m, and the westerly flow at 3 km height was more intense in M05m. This westerly flow at 3 km height increased the evaporation of the rain droplets, thus intensifying the cold pool. These airflows, that is, the high-θe low-level inflow and the mid-level westerly flow, created conditions favorable for intense convection. On the other hand, in M02p, the rainfall was relatively weak and it was not organized into a line shaped band. These features of M02p resulted from a low-level inflow of low-θe air and a weak mid-level airflow. These rainfall structure analysis results indicate that the different environmental conditions in each member were responsible for the different types of rainfall system produced.

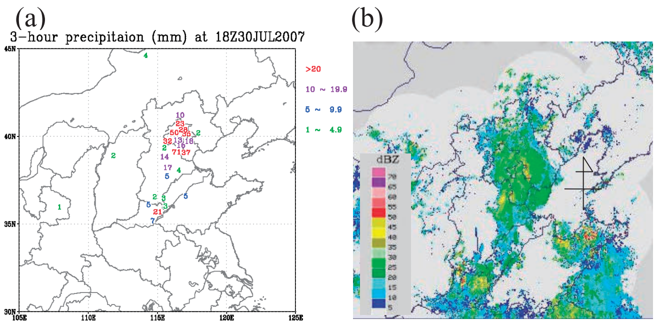

Fig. D-8-2. (a) Distribution of 3-hour rainfall at 18 UTC on 30 July 2007. (b) Reflectivity distribution at 18 UTC. Both figures are from the CMA website.

c) Comparison with Tier-1 experiments

Do these downscale experiments contain more information than the Tier 1 experiments? Data with a grid point interval of 15 km were produced from the Tier 2 output, and then compared with the Tier 1 results. Figure D-8-3 shows the 3-hour rainfall distributions produced by the Tier 1 and Tier 2 experiments. The shapes of the rainfall systems reproduced by the Tier 2 experiments were similar to those reproduced by the Tier 1 experiments. This similarity is attributable to the environmental and boundary conditions. Because the Tier 2 boundary conditions were produced by interpolation of the Tier 1 output, it is reasonable that the position of intense convergence in the Tier 2 results should be roughly similar to that in the Tier 1 experiments. The Tier 2 environmental conditions were also similar to those of Tier 1. Thus, the vertical shear of the horizontal wind and the θe value of the low-level inflow were not changed by the interpolation. As a result, the Tier 2 experiments reproduced the same type of convective system as the Tier 1 experiments.

Next, rainfall amounts were compared between the Tier 2 and Tier 1 results. The Tier 2 rainfall amounts were similar to those of Tier 1, except in M04p (Fig. D-8-4a). This similarity suggests that rainfall amounts were also controlled by the boundary conditions. On the other hand, the maximum Tier 2 rainfall amounts were larger than the maximum Tier 1 amounts (Fig. D-8-4b), and the region with rainfall exceeding 1 mm in 3 hours was smaller in Tier 2 than in Tier 1 (Fig. D-8-4c). These

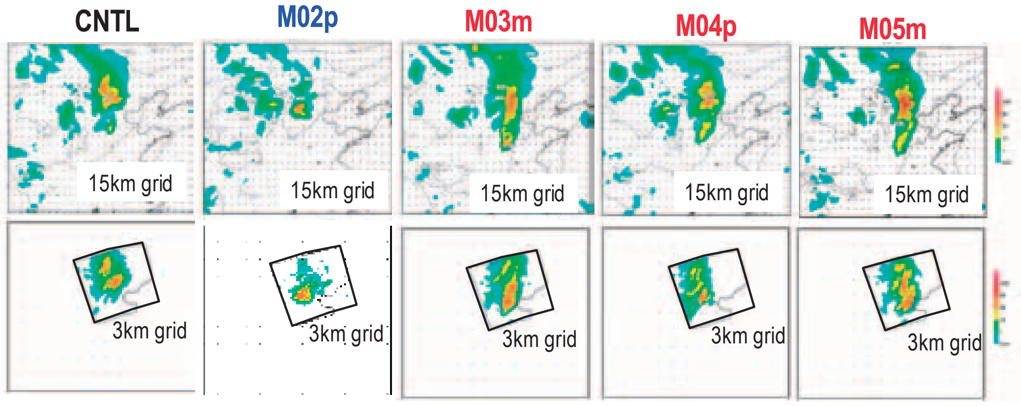

Fig. D-8-3. Three-hour rainfall distributions in the Tier 1 (top) and Tier 2 (bottom) experiments. The rectangular areas in the lower panels indicate the model domain of the Tier 2 experiments.

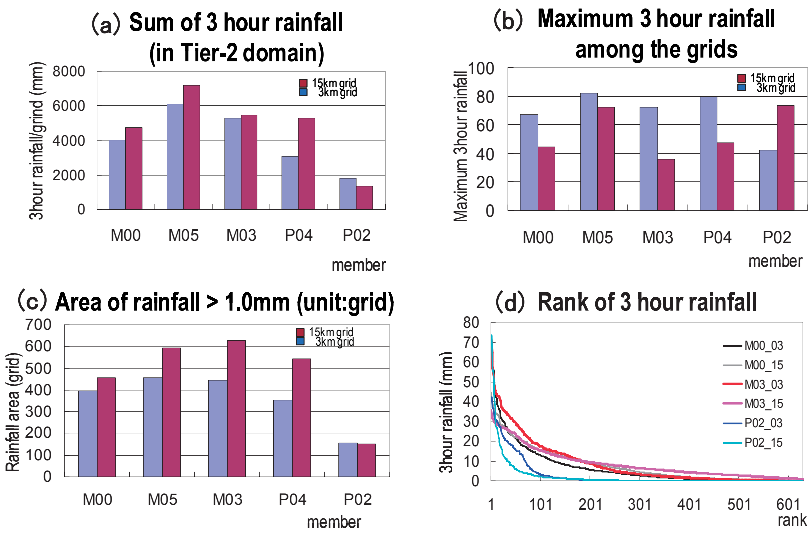

Fig. D-8-4. Comparison of rainfall between the Tier 1 (15 km) and Tier 2 (3 km) experiments. (a) Total 3-hour rainfall, (b) maximum 3-hour rainfall, and (c) the area in which the 3-hour rainfall exceeded 1.0 mm. (d) Ranking of 3-hour rainfalls. The rainfall rank is shown on the horizontal axis.

results indicate that Tier 2 rainfalls were more concentrated than those of Tier 1. This result is supported by the rainfall amount ranking (Fig. D-8-4d). Because the maximum rainfall is important for the prediction of heavy rainfalls, the relation between the model resolution and the rainfall concentration should be investigated further.